First-principles simulations of STM images: From tunneling to the contact regime

Jose Manuel Blanco,[1] Cesar González,[1] Pavel Jelínek,[1,2] José Ortega,[1] Fernando Flores,[1] and Rubén Pérez[1]
[1]*Departamento de Física Teórica de la Materia Condensada, Universidad Autónoma de Madrid, E-28049 Spain*
[2]*Institute of Physics, Academy of Sciences of the Czech Republic, Cukrovarnická 10, 1862 53, Prague, Czech Republic*
(Received 27 January 2004; published 9 August 2004)

The operation of the STM on metallic surfaces from the tunneling to the contact regime has been explored with a combination of first-principles total energy methods and a calculation of the electronic currents based on nonequilibrium Keldish-Green's function techniques. Our calculations for the behavior of the total energy, forces, atomic relaxations, and currents for an Al tip on an Al(111) surface as a function of the tip-sample distance indicate that atomic relaxations and saturation effects become relevant in a similar distance range where the onset of a short-range chemical interaction between the tip apex and the surface atoms is taking place. These two factors, that have an opposite influence in the current, lead to corrugations of the order of 0.2 Å, similar to the ones found experimentally in other (111) metal surfaces, for the closer distances (around 4.25 Å) where stable operation can be achieved.

DOI: 10.1103/PhysRevB.70.085405 PACS number(s): 68.37.Ef, 71.15.Mb, 73.40.Gk

I. INTRODUCTION

Scanning tunneling microscopy (STM)[1] has led to a revolution in the study of the structure and electronic properties of conducting (semiconductor and metal) surfaces and adsorbates. However, STM does not give a direct image of the atomic geometry of the surface but it rather maps the electronic structure.[2] For example, an oxygen atom adsorbed on a metal surface is seen as a depression on the STM image.[3] The interpretation of STM images is mostly based on the early development by Tersoff and Hamman (TH)[4] of a simple theory for the low-bias experimental images. Based on severe approximations for the tip electronic structure and the tunneling process (see later), they showed that the tunneling current is proportional to the local density of states of the sample at the Fermi level evaluated at the position of the tip apex.

This simple approach provides a quick, qualitative understanding of many experimental images, but fails to reproduce the quantitative details. For example, the corrugation measured on close-packed metallic surfaces[5,6] is an order of magnitude larger than the one predicted by the TH theory (see, for example, Refs. 2, 7, and 8). These discrepancies have to be related to the crude approximations involved in the TH approach: (1) Assume no change in the structure and electronic properties of the tip and sample due to their mutual influence, (2) a simplified electronic structure for the tip (TH assumes an *s* wave while *d* orbitals have a significant contribution at the Fermi level for typical W or Pt tips that can play a role in STM imaging),[7] and (3) the use of a first order perturbative approach for the tunneling process. These assumptions are specially questionable for low tunneling resistance images, where tip-sample distances are shorter (below 5 Å, closer than expected in the early days), and multiple scattering events are relevant. Furthermore, recent work shows that, under those conditions, relaxations induced both in the tip and the sample due to the tip-sample interaction can lead to the modification of the relative stability of different adsorption sites.[9] In this latter case, density functional theory (DFT) calculations are crucial to understand the conflicting evidence provided by low-energy electron diffraction and STM for the coverage and adsorption site of highly mobile adsorbates.

The earlier discussion strongly calls for a theoretical approach capable to handle at the same time a sophisticated description of the electronic structure of the system and a rigorous nonequilibrium nonperturbative treatment of the tunneling process. Few studies have combined in the past standard first-principles electronic structure methods based on extended orbital basis [plane waves (PW),[10] linear muffin-tin orbital,[11] projector augmented waves][12] with a scattering formalism for the current. These approaches were limited by the severe restrictions in the description of the geometries of the tip and sample imposed by the symmetry requirements in order to keep the calculation feasible (in some cases, the tip is not even atomically described but modeled by simple potentials).[12] Corbel *et al.*[13] developed a more flexible scheme that combines a multiple scattering formalism,[14,15] where only transfer matrix elements between tip and sample bulk states are considered, with first-principles calculations for the relevant fragments of the hamiltonian of the whole system. They were able to describe the atomic structure of tip and sample but they did not consider the effect of the atomic deformations induced by the tip-sample interaction. This effect has been recently taken into account by Hofer *et al.*,[16] combining a first-principles pseudopotential approach to determine the tip and surface structure with Bardeen's perturbation theory for the calculation of the tunneling current between the relevant tip and sample wave functions obtained from independent calculations.

In this paper, we combine standard *ab initio* plane wave pseudopotential methods for the determination of the atomic relaxations induced in the tip and sample by their mutual interaction, with a calculation of STM currents based on nonequilibrium Keldish-Green's function techniques.[17] The connection between the structural and transport calculations is done through a fast local-orbital DFT technique (FIREBALL2003),[18] that efficiently maps the electronic hamiltonian determined from the PW calculation, and can be natu-

rally linked with the transport formalism, that is expressed in terms of localized orbitals.

Using this approach, we perform a detailed study of the currents from the tunneling to the contact regime. The large tunneling resistance limit provides a stringent test on the convergence with system size of the tunneling currents and validates our approach. In the low tunneling resistance regime, these calculations allow us to explore the interplay between the current increase due to the atomic relaxations and the saturation effects (due to multiple scattering processes) in the value of the current, not considered previously.[16]

We have focused our analysis on Al(111) surfaces, where extremely large corrugations have been reported, and tentatively attributed to large tip-induced surface relaxations.[5] Our results for an Al(111) surface and an Al tip indicate that the presence of both significant atomic relaxations and saturation effects in the current are associated with the onset of a chemical interaction between the tip apex and the surface atoms, and become relevant in a similar distance range. As these two effects tend to compensate, calculations including all the hopping processes are needed in order to validate previous claims of the role of atomic relaxations in the explanation of the measured corrugation amplitudes.[16] In the case of Al(111), we found corrugations of the order of 0.2 Å, similar to the ones found in other (111) metal surfaces. The atomic relaxations and the conductance between an Al tip (modeled by a single atom) and an Al(110) surface have been explored by Di Ventra and Pantelides[19] but for distances between 1.3 and 3.3 Å, that fall out of the distance regime considered in this work.

The rest of the paper is organized as follows. In Sec. II, we present our theoretical description for the calculation of the atomic relaxations induced by the tip-sample interaction, including the model for the tip and sample we are going to consider. The presentation of the Keldish-Green's function method we use for obtaining the electronic conductance and the discussion and validation of our particular implementation (including the mapping of the electronic hamiltonian in a local basis and convergence issues) is covered in Sec. III. Section IV is devoted to the characterization of the atomic relaxations induced in the tip and sample by their mutual interaction along the approaching paths on different points of high symmetry in the surface. The distance dependence of well converged calculated currents is analyzed in Sec. V, with particular emphasis on the interplay between atomic relaxation and saturation effects on the resulting theoretical corrugations. We conclude (Sec. VI) with a comment on the general validity of our results.

II. THEORETICAL MODELING OF THE ATOMIC RELAXATIONS DUE TO THE TIP-SAMPLE INTERACTION

A. Model geometry

Figure 1 shows the initial geometry of the system we consider for the calculation of the tip and sample atomic relaxations due to their mutual interaction: a five-layer Al(111) slab with the correct face-centered-cubic (fcc) stacking and a tip, represented by a pyramid with four Al atoms, attached to one of the (111) surfaces. W tips prepared by electrochemical etching of tungsten wires and cleaned by field desorption were originally used in the STM experiments on fcc (111) surfaces. The resulting tips are relatively blunt and produce images with a poor resolution. Atomic resolution was only obtained after a large increase in the sample potential by a short time while the surface was scanned.[5,6] This procedure leads to a significant deformation of the scan area in the surface and the lengthening of the tip that can only be explained by a restructuring of the tip that involves material transfer from sample to tip. Our four-atom Al tip mimics the basic characteristics of the low-coordinated metallic cluster resulting from sample contamination that can be expected to be formed at the tip apex.

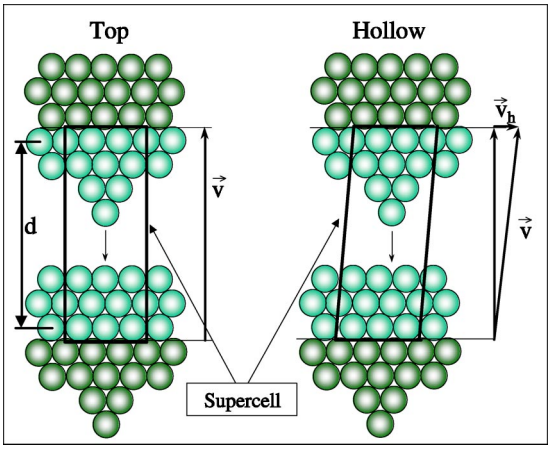

FIG. 1. (Color online) Initial geometry for the supercell [with the four-atom Al tip and the five-layer Al(111) slab] used for the calculation of the atomic relaxations due to the tip-sample interaction. The vector defining the normal periodicity has, in the case of the hollow fcc and hollow hcp sites, also an in-plane component $\vec{v}_h$, adjusted in each step of the approaching process in order to keep the tip on top of one of these different high symmetry positions. An arbitrary constant is substracted to *d*, the distance between the fixed planes, to make the tip-sample distance equal to the normal distance between the tip apex and the topmost surface atoms when the tip and sample are far apart.

In our calculation we introduce a 3×3 periodicity in the direction parallel to the surface, large enough to decouple the different tips from each other. We use a supercell approach, imposing also periodic boundary conditions in the direction perpendicular to the surface. In this way, the tip interacts with the free surface of the slab. The vector defining this last periodicity has, in the case of the hollow fcc and hollow hexagonal-close-packed (hcp) sites, also an in-plane component, adjusted in each step of the approaching process in order to keep the tip on top of one of these different high symmetry positions on the surface (see Fig. 1).

The approaching of the tip to the surface is simulated reducing the normal (out-of-plane) component of the corresponding supercell lattice vector by steps of 0.25 Å. After each step, the system is allowed to relax towards its configuration of minimum energy. In this relaxation, the atoms located in the central three layers of the slab remain fixed. This is a good approximation for small relaxations of the sample

atoms; for small tip-sample distances, these relaxations might be large (see later) and our calculations should be taken as a first approximation to the problem. The tip-sample distance is defined as the distance between these fixed layers in two neighboring slabs (see Fig. 1). An arbitrary constant is substracted in order to make the tip-sample distance equal to the normal distance between the tip apex and the topmost surface atoms when the tip and sample are far apart and there are no induced relaxations. With this definition, variations in the tip-surface distance are directly comparable to the relative displacements of tip and sample which are measured on the vertical piezo scale in the experiments.

B. Total energy DFT calculations

The relaxed structures of the tip and sample due to their mutual interaction have been determined using a standard first-principles total energy code (CASTEP).[20] The energies and forces were calculated within the DFT in its plane-wave pseudopotential formulation.[21] We have used both the local density approximation (LDA) and the gradient corrected approximation[22] (GGA) for the exchange-correlation functional in order to assess their influence in the relaxed structures. Al atoms were described by ultrasoft pseudopotentials.[23] The wave functions were expanded on a mesh of 16 Monkhorst-Pack k points[24] on the two-dimensional first Brillouin zone with a plane-wave cutoff of 140 eV. A smearing width of $\sigma=0.2$ eV was used.[25] The evolution of the total energy and the forces are used to monitor the relaxation. The process is stopped when the changes are less than 10^{-6} eV/atom and 0.01 eV/Å, respectively. The normal force acting on the tip is calculated as a numerical derivative of the energy curve. As very low voltages can be used to image metal surfaces, we have not considered the influence of the electric field in the structure of tip and sample.[2]

III. MODELING TUNNELING CURRENTS

A. Keldish-Green's function method

Our approach for the calculation of the electrical current flowing through the tip-sample system is based on the nonequilibrium Green's function formalism developed by Keldish.[26] Details of the formalism can be found in Ref.17. Here we stress the main points and compare this formulation with other approaches in the literature for the calculation of tunneling currents.

The whole tip-sample system is assumed to be described in an orthogonal local orbital basis. This leads to an effective tight-binding hamiltonian that can be parametrized, as has been done in the past, or calculated from first-principles calculations as described later at each point of the approaching path. Having in mind the application to the STM simulations, it is advantageous to rewrite this hamiltonian as the sum of three terms: $\hat{H}=\hat{H}_s+\hat{H}_t+\hat{H}_{ts}$, with one term associated with the sample (s), one with the tip (t), and finally a term that takes into account the interaction between tip and sample. Notice that this interaction is simply described by the hopping matrix $\hat{T}_{ts}$ (the corresponding box linking the basis orbitals in the tip and sample in the hamiltonian of the whole system). Then, we can write an expression for the tip-sample current that only involves the calculation of the Green functions for the isolated tip and sample and the hopping matrix that couples both parts of the system[17]

$$I=\frac{4\pi e}{\hbar}\int_{-\infty}^{\infty}d\omega \mathrm{Tr}[\hat{T}_{ts}\hat{\rho}_{ss}(\omega)\hat{D}^r_{ss}(\omega)\hat{T}_{st}\hat{\rho}_{tt}(\omega)\hat{D}^a_{tt}(\omega)] \times[f_t(\omega)-f_s(\omega)], \quad (1)$$

where $f_i(\omega)$ $(i=t,s)$ is the corresponding Fermi-Dirac distribution function, $\hat{\rho}_{tt}$ and $\hat{\rho}_{ss}$ are the density of states matrices associated with the tip and sample, while

$$\hat{D}^r_{ss}=[\hat{1}-\hat{T}_{st}\hat{g}^r_{tt}(\omega)\hat{T}_{ts}\hat{g}^r_{ss}(\omega)]^{-1} \quad (2)$$

and

$$\hat{D}^a_{tt}=[\hat{1}-\hat{T}_{ts}\hat{g}^a_{ss}(\omega)\hat{T}_{st}\hat{g}^a_{tt}(\omega)]^{-1}; \quad (3)$$

where $\hat{g}^r_{tt}$ and $\hat{g}^r_{ss}$ are the retarded and advanced Green function for the tip and sample, respectively. The sum over all the orbitals in the tip and sample have been rewritten in Eq. (1) in terms of the trace (Tr), the sum over the diagonal elements of the corresponding product matrix.

Notice that the denominators $\hat{D}^r_{ss}$ and $\hat{D}^a_{tt}$ take into account the multiple scattering effects via the summation up to all orders of an expansion of the scattering matrices $\hat{X}^A=\hat{T}_{ts}\hat{g}^a_{ss}(\omega)\hat{T}_{st}\hat{g}^a_{tt}(\omega)$ and $\hat{X}^R=\hat{T}_{st}\hat{g}^r_{tt}(\omega)\hat{T}_{ts}\hat{g}^r_{ss}(\omega)$, and are responsible for the saturation of the tunneling current found for small tip-sample distances (see the discussion later).

We can easily make contact with other multiple-scattering approaches[12,13] developed for the calculation of STM currents that are based in the Landauer formalism.[27] In the low tip-sample bias case (the only one discussed in detail in this work), the relevant quantity is the differential conductance $G=dI/dV$, that is given by

$$G=\frac{4\pi e^2}{\hbar}\mathrm{Tr}[\hat{T}_{ts}\hat{\rho}_{ss}(E_F)\hat{D}^r_{ss}(E_F)\hat{T}_{st}\hat{\rho}_{tt}(E_F)\hat{D}^a_{tt}(E_F)]. \quad (4)$$

This expression can be rewritten in a form that closely resembles the Landauer equation

$$G=\frac{dI}{dV}=\frac{2e^2}{h}\mathrm{Tr}[\hat{t}\hat{t}^+], \quad (5)$$

where $\hat{t}=2\pi\hat{\rho}^{1/2}_{tt}\hat{D}^a_{tt}\hat{T}_{ts}\hat{\rho}^{1/2}_{ss}$ and use of the cyclic property of the trace has been done. Notice that $\hat{t}$ defines the transfer matrix of the system and we can analyze the contribution of the different channels to the differential conductance by diagonalizing it.

Compared with the standard formulation for those transmission coefficients in terms of the Green's function of the whole tip-sample system and the self-energies representing the coupling with the corresponding reservoirs, our approach shows explicitly the dependence with the Green's functions of the different fragments, each of them coupled to its own reservoir, and the coupling between these fragments. Notice that those Green's functions are easy to calculate in practice

as the fixed metallic layers in the slab (with two-dimensional periodicity) (see Sec. III B) are enough to provide the infinite number of channels needed to represent the corresponding electrodes. The additional flexibility introduced by this decomposition into the tip and sample subsystems can be also particularly useful when simple approximations can be made to the tip-sample coupling, as discussed later.

Notice that, although we find the combination with the FIREBALL code particularly efficient (see Secs. III B and III C), the formulation for the STM simulations presented here can be easily implemented with any other local orbital code. Closely related approaches, based on the combination of *ab initio* calculations on local-orbital basis and Keldysh-Green function methods, have been recently applied to study transport properties in nanocontacts.[28–32]

B. Mapping the electronic hamiltonian in a local basis: FIREBALL

The connection between the structural and transport calculations is done through a fast local-orbital DFT technique (FIREBALL2003),[18] that efficiently maps the electronic hamiltonian determined from the DFT-PW calculation, and can be naturally linked with the transport formalism described earlier, that is expressed in terms of localized orbitals.

In FIREBALL, the valence wave functions are expanded in a set of strictly localized pseudoatomic orbitals (they are exactly zero for distances larger than the cutoff radius r_c). This offers a very favorable accuracy/efficiency balance if the atomic-like basis set is chosen carefully. We have used a minimal basis that includes *s* and *p* orbitals for Al with a cutoff radii $R_c = 6.4$ a.u., and provides values for the lattice parameter and the bulk modulus of fcc Al ($A = 3.97$ Å, $B = 74$ GPa), identical to the results of the PW code CASTEP and in good agreement with the experiment ($A = 4.05$ Å, $B = 76$ GPa).

The ability of the FIREBALL code to reproduce, with a properly chosen minimal basis, the results of fully converged first-principles calculations has been extensively checked in a number of systems against fully converged plane-wave DFT calculations (see, for example, Refs. 33 and 34). Notice, in particular, the tests that we have performed in our recent study of the mechanical properties and electrical conductance during the stretching and final breaking of Al nanocontacts.[35] Those results indicate that we could have used FIREBALL, not just as a way to map the PW results in a local basis, but as the total energy method to calculate the structure of the tip and sample during the approach. However, in order to rule out any inaccuracy in the determination of the onset of the tip and sample relaxations and to compare the influence of the exchange-correlation functional use, we have decided to perform the calculation of the relaxed structures with the fully converged PW code.

C. Simulating STM currents: Practical implementation and convergence issues

The proper simulation of the STM images on a close-packed metal surface like Al(111) requires to go beyond the model considered for the calculation of the tip and surface relaxations. While, according to our calculations, a slab with five layers is a reasonable model to describe those relaxations (remember our discussion of this point earlier), this finite system does not describe properly the details of the surface density of states. This would reflect, in particular, in the presence of spurious large differences between the tunneling currents calculated for symmetry positions like hcp and fcc that have to be pretty equivalent for large tip-sample distances. These errors can lead to a 100% overestimation of the corrugation when the top and one of the hollow positions are compared, and, even more importantly, to the wrong corrugation vs distance behavior. In our current calculations we have thus considered a slab with 11 layers, where we kept the positions from the total energy calculations for the 5 layer slab and include in between the third and fourth layers six more (111) planes with the correct stacking. Test calculations on a 14 layer slab, where three more bulk layers are included, show that the STM currents and corrugations are already converged with the 11 layer slab (differences are below the numerical accuracy).

The other critical point in the simulation of the STM images is related to the calculation of H_{ts}. During normal STM operation, the average tip-surface distance is assumed to be, depending on the voltage and current conditions, in the range between 4 and 8 Å. It is clear that, in the large distance regime, we cannot use in order to calculate the tip-sample hopping elements the strictly localized pseudoatomic orbitals that are needed to have an accurate and efficient description of the electronic bulk properties, as typical cutoff radii are smaller than the tip-surface distance. In our case, we have determined these hoppings from the calculation of a dimer formed by the corresponding tip and sample atom with the FIREBALL code. In this calculation we have used pseudoatomic orbitals, generated with a cutoff radius larger than 20 a.u., that reproduce the behavior of the real free-atom orbitals and, thus, are able to describe properly the overlap of the tip and sample wave functions. Notice that there is no inconsistency in the fact that we use different basis for the calculations of the different terms in the conductance [see Eq. (5)]. The formulation outlined in the previous section explicitly separates the contributions coming from the "interatomic" matrix elements (those between an atom in the tip and another atom in the sample) that are represented by $\hat{T}_{ts}$ and the "intraatomic" ones that are described through the density of states matrices $\hat{\rho}_{tt}$ and $\hat{\rho}_{ss}$. This separation allows us to concentrate our efforts in the proper calculation of each term. In particular, the charge density matrices have to be calculated from the corresponding tip and sample intraatomic Hamiltonians, that include the structural and electronic effects induced by the mutual interaction between tip and sample at close distances and are properly described by the pseudoatomic basis with the finite cutoff. For large distances, where those effects can be neglected, this approach simplifies significantly the calculation of STM currents as it only requires, apart from the very quick dimer calculation for the hoppings as a function of the distance, two independent (smaller) calculations for tip and sample.

Although the use of the dimer calculation for the determination of the tip-sample hoppings adds flexibility and a sig-

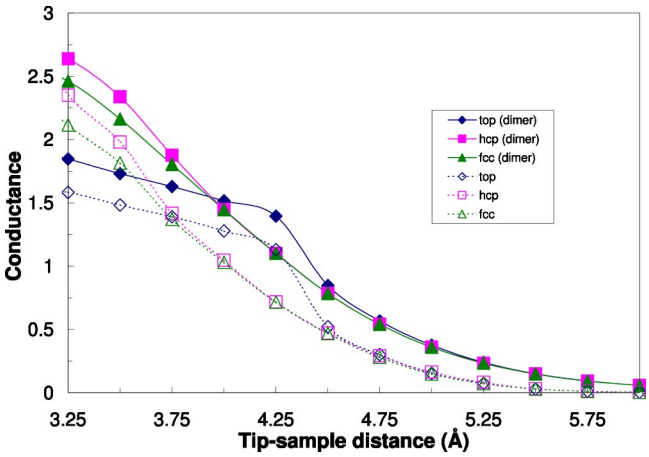

FIG. 2. (Color online) Conductance (in units of $2e^2/h$) as a function of the tip-sample distance for the different symmetry positions (top, fcc, and hcp) in the Al(111) surface. Two different schemes for the calculation of the tip-sample hoppings are compared: fully self-consistent calculation (with strictly localized pseudoatomic orbitals, $R_c = 6.4$ a.u.) of the whole system (empty symbols), and a dimer calculation with the real free-atom orbitals.

nificant speed-up to the STM calculation, it is based on an approximation that has to be validated. The hoppings calculated in this way include the dominant orthogonalization effects of the corresponding two atoms but not the orthogonalization and electrostatic potential contributions coming from the rest of the atoms in the tip and sample. For the short distance range, where we can expect those effects to be particularly important, we have checked the influence of those contributions in the STM currents. For that, we have compared the conductances obtained with the dimer approximation and those calculated using the real hopping elements that appear in the final selfconsistent Hamiltonian for the whole tip-sample system (see Fig. 2).

These calculations show that, for distances smaller than 4.75 Å, although absolute values of the conductance differ due to the different cutoff radii for the orbitals used in both cases,[13] the two approaches produce for the different symmetry positions, conductance versus distance curves that have the same shape, leading in both cases to the correct distance behavior of the corrugation and quantitative differences in the estimated corrugation smaller than 2.5%. Larger corrugations correspond to the calculation with the full Hamiltonian (0.29 vs 0.22 Å for the maximum value, as discussed in Sec. V), where the orbitals with shorter range are considered. This increase in the corrugation with the use of more localized basis sets have also been described in STM simulations with semiempirical matrix elements.[15] For larger distances, orthogonalization effects are negligible and the different decay behavior in the conductance is related to the different extension of the orbitals considered in each calculation (extended free-atom-like orbitals for the dimer calculation and localized pseudoatomic orbitals with cutoff radius equal to 6.4 a.u. in the hoppings in the final self-consistent Hamiltonian).

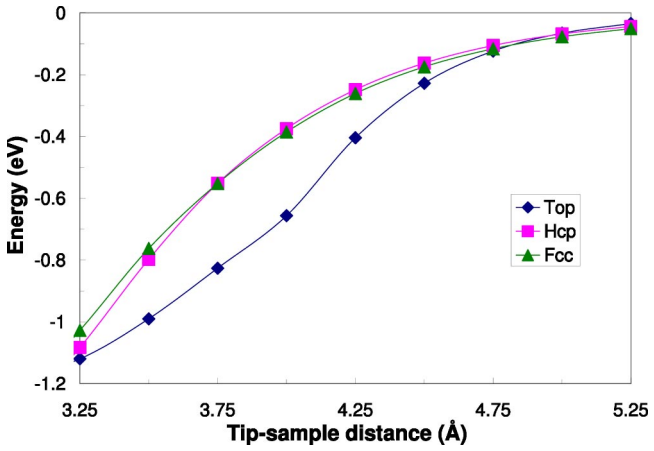

FIG. 3. (Color online) Total energy, calculated with the DFT-LDA approximation, as a function of the tip-sample distance approaching the tip on top of three different high symmetry positions (top, hollow fcc, and hollow hcp) in the Al(111) surface.

IV. TIP-SAMPLE RELAXATIONS DURING THEIR APPROACH

The nature and strength of the short-range tip-sample interaction for the tip approaching the surface in three different symmetry positions (top, hollow fcc, and hollow hcp) can be characterized through the analysis of the total energies (summarized in Fig. 3), the tip-sample forces (see Fig. 4) and the atomic relaxations induced (monitored through the apex-surface distance in Fig. 5). These data correspond to the system with the five-layer slab, where the three central layers are kept fixed during the atomic relaxation for each step of the approaching process (see Fig. 1). In Fig. 3 and subsequent figures the results are plotted as a function of the "tip-surface distance" defined in Sec. II A. Remember that, with this definition, variations in the tip-surface distance are directly comparable to the relative displacements of tip and sample as measured on the vertical piezoscale in the experiments.

Total energies already show the marked differences between the top and the two hollow positions considered. The

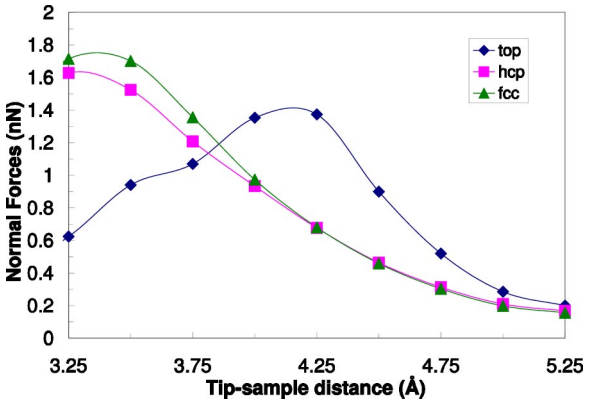

FIG. 4. (Color online) Forces, calculated with the DFT-LDA approximation, as a function of the tip-sample distance approaching the tip on top of three different high symmetry positions (top, hollow fcc, and hollow hcp) in the Al(111) surface.

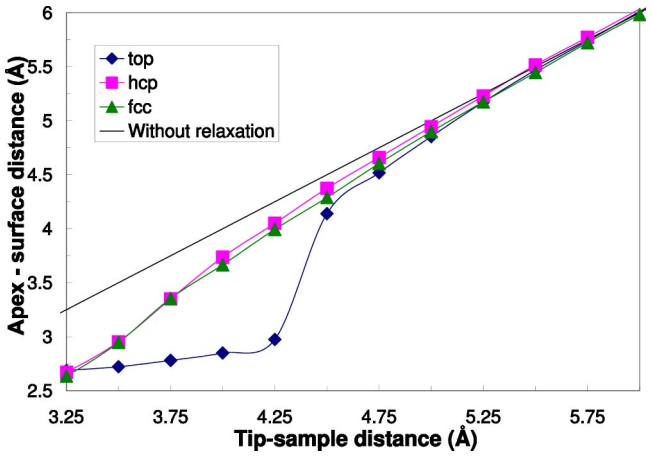

FIG. 5. (Color online) Apex-surface distance as a function of the tip-sample distance for different symmetry positions in the Al(111) surface. The straight line shows the apex-surface atom distance if no relaxations of tip and sample were allowed. The faster change in the top case is mainly due to the upwards displacement of the surface atom below the tip.

three curves are very similar till a distance of 4.75 Å, where the energy of the top position starts to increase significantly. This departure can be correlated with the onset of significant tip-sample forces (see Fig. 4) and relaxations induced in tip and sample, that are particularly large in the range 4.25–4.50 Å, where the apex-sample distance decreases by 1.17 Å (see Fig. 5) leading to the formation of a strong covalent bond between the two atoms.

This distance reduction is mainly due to the upwards displacement, by approximately 0.9 Å, of the Al atom right below the tip. Notice that, before that point, the relaxations induced in both the surface adatom and the tip apex are quite symmetric and of the order of 0.1 Å. For distances smaller than 4 Å, the surface atom is pushed back towards the surface, keeping the bond with the apex atom, that also relaxes back to the initial tip configuration. These atomic displacements lead to a slow decrease of the apex-surface distance, which is close to the Al bulk n.n. distance (2.80 Å).

The two hollow positions present a different behavior. Relaxations on the surface atoms are modest (below 0.05 Å at 4.5 Å), reaching a maximum value of 0.2 Å for a tip-surface distance of 3.3 Å, while the position of the apex atom changes 0.4 Å at that same distance.

It is worth mentioning that the tip-sample forces increase significantly for distances smaller than 4.75 Å in the top position. This force presents a maximum for $d=4.25$ Å, a distance for which the microscope operation might be mechanically unstable.[36] For the hollow positions, this maximum appears for $d\simeq 3.25-3.5$ Å. It is clear that, due to the mechanical instability of the interface (see later), corrugations can only be measured for distances larger than 4.25 Å.

Similar results have been found in previous studies of the interaction of tips and metallic surfaces. Regarding the atomic relaxations, the behavior we observe for the top position agrees quite well (in the absolute value of the relaxations of the apex and the surface atom, and in the relevant tip-sample distance range) with the results of Hofer *et al.*[16] for a four-atom W tip and a five-layer slab of Au(111) planes. However, we do not see the even larger tip and sample relaxations that they have reported for the hollow position.

Total energies and normal forces acting on the tip can be qualitatively compared with those found by Dieska *et al.*[37] for a Cu(111) surface interacting with a Si tip. In these calculations, energies and forces for top and hollow positions present a behavior very similar to the one found in this work. The maximum normal force values [approximately 1.5 (1.8) nN for top (hollow) in our case] are of the same order of those found in Ref. 37 (around 2 nN).

Given the well-known deficiencies of the LDA approximation describing weak bonds, it seems necessary to check that the main conclusions of our analysis, and, in particular, the relevant distance range and absolute value of the induced relaxations are not sensitive to the exchange-correlation functional used. We have repeated the calculation of the total-energy as a function of the tip-sample distance with the GGA approximation for the top position. Our results show that the two energy curves are very similar, apart from an almost rigid small shift in the energy (substracting the corresponding total energy values at 5 Å, the two curves fall one on top of the other). The onset of significant relaxations and the value of the atomic displacements are also very close in both calculations.

V. WELL CONVERGED TUNNELING CURRENTS AND CORRUGATIONS: COMPARISON WITH THE EXPERIMENT

As STM experiments on metal surfaces are usually done with small bias voltages (less than 100 meV), the conductance provides a good characterization of the system: Comparison with experiments at different bias conditions are easy, as the theoretical current can be simply estimated as the product of the conductance and the bias voltage. On the other hand, the values of conductance, particularly when written in terms of its quantum unit $G_0=2e^2/h$, provide insight into the relation between the structure of the system and its electronic transport properties. The values of the conductance as a function of the tip-surface distance for the three symmetry positions considered in our study are shown in Fig. 6. We are covering here the different relevant regimes, showing in particular the transition between the tunneling and the contact regions.

These curves already reflect the role of the tip and sample relaxations, as the conductance of the top and hollow positions become markedly different in the distance range where those relaxations start to be significant for the top position. However, there are other effects, including multiple scattering effects, that have an important role in determining the final value of the conductance. Figure 7 helps to quantify the contribution of these different factors comparing the final curves for the top and fcc positions with those where either the multiple scattering or the induced relaxations are not included. Multiple scattering effects start to play a role for distances below 5 Å, but they become particularly relevant for the distance range where relaxations take place: If they are not included both the values of the conductance and the

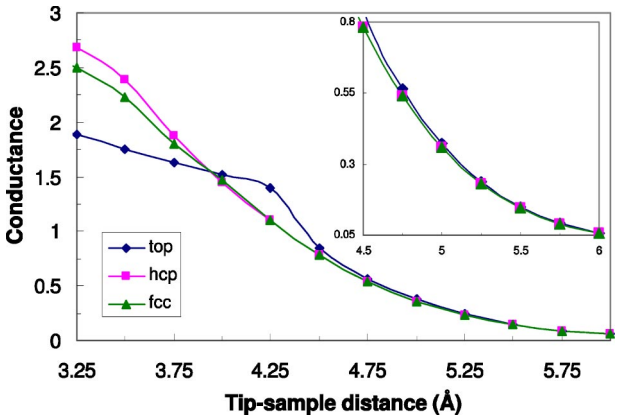

FIG. 6. (Color online) Conductance (in units of $2e^2/h$) as a function of the tip-sample distance for the different symmetry positions (top, fcc, and hcp) in the Al(111) surface. The curves for the three positions tend to merge rapidly as we increase the tip-sample distance, resulting in a very small normal corrugation (see inset).

differences between different positions in the surface are grossly overestimated. Notice, in particular, that these conductance values would lead to an overestimation of the surface corrugation calculated theoretically. On the other hand, the proper calculation (including multiple scattering) for an ideal tip and sample (where we keep their structure when they are far apart for the whole distance range) shows that relaxations play the crucial role in the differences observed between the top and hollow positions.

Before discussing the implications of these conductance results for the corrugations observed as a function of the tip-sample distance, it is interesting to compare these results with those published in the literature for other metallic systems.

In the pure tunneling regime, where relaxations do not play an important role, our results can be compared with other calculations where the tip and surface electronic properties have been determined by *ab initio* methods, like those

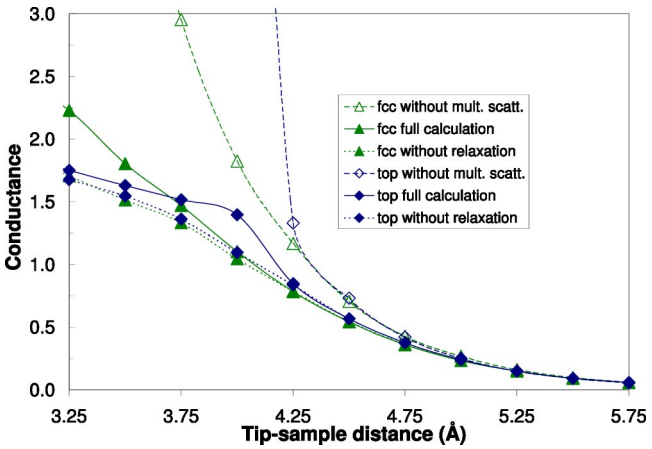

FIG. 7. (Color online) Conductance (in units of $2e^2/h$) as a function of the tip-sample distance for the top and fcc positions, showing the effects of multiple scattering and atomic relaxations.

presented by Hofer *et al.*[16] for a W tip on a Au(111) surface and Corbel *et al.*[13] for a Cu tip on a Cu(001) surface. In the case of W on Au(111), they have used a simple Bardeen approach where the wave functions from independent tip and sample calculations are used to calculate the tunneling currents. The conductance at the largest distance considered in that calculation (5 Å) can be estimated from the currents (see Fig. 3 in Ref. 16 and the bias considered, −0.1 V). This gives a value of $0.3\times10^{-3}G_0$, that is roughly three orders of magnitude smaller than our result for the Al tip on Al(111) surface for that same distance. We believe that part of this discrepancy is due to the Bardeen's model used in Ref. 16: image potential effects would reduce considerably the tunneling barrier and would increase by one or two orders of magnitude the tunneling current.[38] In our approach, the appropriate behavior of the tunneling currents is included as shown by the saturation currents we find when the tip-sample distance is small (around 3.5 Å).[39] However, as discussed later, corrugation values for the relevant distance regime are of the same order (0.2 Å) in both our calculations and those of Ref. 16. The approach for the current calculations by Corbel *et al.* for a Cu tip on Cu(001)[13] is more similar to our work, as they used a Landauer approach combined with scattering techniques to calculate the transmission coefficient, and the scattering matrix is determined using Green's function techniques. The self-consistent hamiltonian is determined on a localized orbital basis set of Slater-type orbitals using the ADF-BAND program. In this case, the conductance values (e.g., 0.01 G_0 for $d=5.6$ Å, see Fig. 5 in Ref. 13) are a factor of 10 smaller than our results for an Al tip on Al(111). These differences in the absolute value of the conductance could be related to the different nature of the atoms involved, if we recall the atomic-like nature of the tip apex and the significant contribution of extended *p* states in the Al atom, as opposed to the *s* states that are dominant in the case of Cu. Our results for the behavior of the conductance in the long distance tunneling regime also agree with those of Corbel *et al.* We observe an exponential decay with a slope value, $d\log_{10}\sigma/dz$, of −0.82 (a reduction by a factor of ten in 1.2 Å), close to the one found in experiments and calculations for other metallic surfaces [$\sim-(0.9-1)$]. For the interesting small resistance regime (tip-sample distances of 3–5 Å), relaxations are not included in the calculation of Ref.13. Nevertheless, we can compare with our results in Fig. 7 for the case with no relaxations. Both calculations show a smooth evolution of the conductance, with no marked differences between the different symmetry positions in the surface, leading to quite small corrugations. This further confirms the important role of tip and sample relaxations in the observed corrugations.

Finally, we consider the influence on the corrugation of the STM images of the tip and sample relaxations induced by their mutual interaction. The corrugation, defined as the height difference between the top and hollow positions in a constant current image, can be extracted from the corresponding current versus distance curves for these two sites (see Fig. 6). The evolution of the corrugation as a function of the tip-sample distance is displayed in Fig. 8. These results

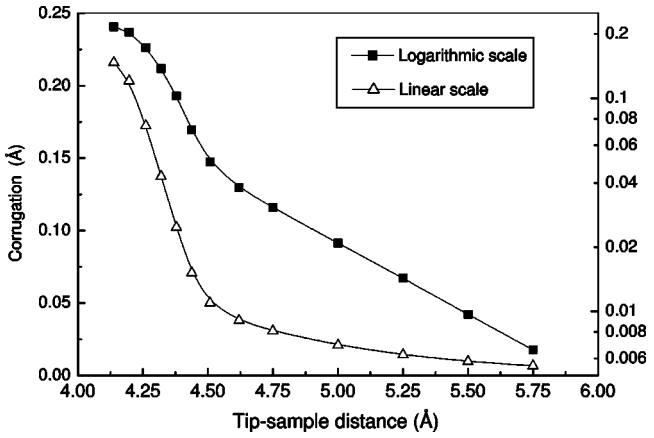

FIG. 8. Corrugation as a function of the tip-sample distance both in a linear (left) and logarithmic (right) scale, in the Al(111) surface.

show that, in the high resistance tunneling regime (tip-sample distances larger than 4.75 Å), the corrugation has a simple exponential behavior, decreasing by a factor of 5 in 1 Å. Below that distance, the tip and sample relaxations produce a complicated behavior in the corrugation. The important tip and sample relaxations induced in the top position for distances smaller than 4.75 Å produce a significant change in the exponential behavior of the corrugation, that increases from 0.05 to 0.175 Å when the tip-sample distance is reduced from 4.5 to 4.25 Å. For smaller distances, the corrugation tends to saturate and reaches a maximum of 0.225 to around 4.13 Å.

According to these results, corrugations of a few hundredths of an angstrom are characteristic of metallic surfaces in the high resistance regime (where no significant relaxations are taking place). Similar values have been reported in other theoretical calculations.[13] Larger corrugations, of the order of a few tenths of an angstrom, are associated with the atomic relaxations induced by the tip-sample interaction. Notice that corrugations of the order of 0.2 Å have also been attributed to tip and sample relaxations in the case of a W tip on an Au(111) surface,[16] and have been measured experimentally in certain close-packed fcc surfaces.[5,6]

In the particular case of Al(111),[5] while most of the corrugation amplitudes measured lie in the range 0.1–0.4 Å, depending on tunneling conditions, corrugations as large as 0.8 Å have also been reported. These high-resolution conditions are very unstable and the tip often undergoes irreversible changes. From our calculations (see Fig. 4) we deduce that those instabilities should appear for distances close to the maximum of the force ($d \simeq 3.5$–4.25 Å). It is clear that relaxations and forces due to the tip-sample interaction depend significantly on the tip structure. While we cannot explain the large corrugations with our tip model, we cannot rule out that a more realistic description of the tip state after the experimental treatment, with a loosely bound atom or small metallic cluster at the apex, could lead to a stable operation with a significant enhancement of the corrugation. These soft modes of the tip apex have also been suggested to explain the large energy dissipation observed during some frequency-modulation atomic force microscopy experiments.[40]

VI. CONCLUSIONS

The operation of the STM on metallic Al(111) surfaces from the tunneling to the contact regime has been explored with a combination of first-principles total energy methods for the determination of the atomic relaxations induced in the tip and sample by their mutual interaction, and a calculation of the electronic currents based on nonequilibrium Keldish-Green's function techniques. This approach overcomes the limitations of all the previous studies, providing at the same time an accurate description of the structure and electronic properties of the tip-sample system with a proper description of the tunneling process, that includes, in particular, multiple scattering effects that become relevant in the low resistance tunneling regime and lead to the saturation of the current.

We have shown that our alternative formulation of the current in terms of the tip and sample subsystems can be exploited to achieve an efficient practical implementation based on a dimer approximation for the corresponding tip-sample coupling. This approach reproduces the expected decay behavior of the current and the corrugations in the large tunneling resistance limit and includes properly the relevant chemical bonding effects in the low resistance limit.

Our calculations for the behavior of the total energy, forces, atomic relaxations, and currents as a function of the tip-sample distance for an Al tip on different symmetry positions (top, fcc, hcp) on an Al(111) surface allow us to determine the expected maximum corrugation and the mechanical stability of the different regimes of operation.

Our results indicate that atomic relaxations and saturation effects become relevant in a similar distance range where the onset of a short-range chemical interaction between the tip apex and the surface atoms is taking place. We expect this behavior to be common to all of the metallic surfaces. These two factors, that have an opposite influence in the current, lead to corrugations of the order of 0.2 Å, similar to the ones found experimentally in other (111) metal surfaces, for the closer distances (around 4.25 Å) where stable operation can be achieved.

ACKNOWLEDGMENTS

P.J. gratefully acknowledges financial support from the FP5 Network HPRN-CT-2000-00154 and by the Spanish Ministerio de Educacion, Cultura y Deportes. This work has been supported by the DGI-MCyT (Spain) under Contract Nos. MAT2001-0665 and MAT2002-01534.

[1] G. Binnig, H. Rohrer, Ch. Gerber, and E. Weibel, Phys. Rev. Lett. **49**, 57 (1982).
[2] W. A. Hofer, Adam S. Foster, and A. L. Shluger, Rev. Mod. Phys. **75**, 1287 (2003).
[3] P. Sautet, Chem. Rev. (Washington, D.C.) **97**, 1097 (1997).
[4] J. Tersoff and D. R. Hammann, Phys. Rev. B **31**, 805 (1985).
[5] J. Wintterlin, J. Wiechers, H. Brune, T. Gritsch, H. Höfer, and R. J. Behm, Phys. Rev. Lett. **62**, 59 (1989).
[6] V. M. Hallmark, S. Chiang, J. F. Rabolt, J. D. Swalen, and R. J. Wilson, Phys. Rev. Lett. **59**, 2879 (1987).
[7] C. J. Chen, Phys. Rev. Lett. **65**, 448 (1990).
[8] C. J. Chen, *Introduction to Scanning Tunneling Microscopy* (Oxford University, Oxford, 1993).
[9] C. Klein, A. Eichler, E. L. D. Hebenstreit, G. Pauer, R. Koller, A. Winkler, M. Schmid, and P. Varga, Phys. Rev. Lett. **90**, 176101 (2003).
[10] K. Hirose and M. Tsukada, Phys. Rev. Lett. **73**, 150 (1994).
[11] G. Doyen, D. Drakova, and M. Scheffler, Phys. Rev. B **47**, 9778 (1993).
[12] H. Ness and A. J. Fisher, Phys. Rev. Lett. **56**, 12 469 (1997).
[13] S. Corbel, J. Cerda, and P. Sautet, Phys. Rev. B **60**, 1989 (1999).
[14] P. Sautet and C. Joachim, Phys. Rev. B **38**, 12 238 (1988).
[15] J. Cerda, M. A. Van Hove, P. Sautet, and M. Salmeron, Phys. Rev. B **56**, 15 885 (1997).
[16] A. W. Hofer, A. J. Fisher, R. A. Wolkow, and P. Grütter, Phys. Rev. Lett. **87**, 236104 (2001).
[17] N. Mingo, L. Jurczyszyn, F. J. Garcia-Vidal, R. Saiz-Pardo, P. L. de Andres, F. Flores, S. Y. Wu, and W. More, Phys. Rev. B **54**, 2225 (1996).
[18] J. P. Lewis, K. R. Glaeseman, G. A. Voth, J. Fritsch, A. A. Demkov, J. Ortega, and O.F. Sankey, Phys. Rev. B **64**, 195103 (2001); P. Jelinek *et al.* (unpublished).
[19] M. Di Ventra and S. T. Pantelides, Phys. Rev. B **59**, R5320 (1999).
[20] CASTEP 4.2 Academic version, licensed under the UKCP-MSI Agreement, 1999.
[21] M. C. Payne, M. P. Teter, D. C. Allan, T. A. Arias, and J. D. Joannopoulos, Rev. Mod. Phys. **64**, 1045 (1992).
[22] J. P. Perdew, J. A. Chevary, S. H. Vosko, K. A. Jackson, M. R. Pederson, D. J. Singh, and C. Fiolhais, Phys. Rev. B **46**, 6671 (1992).
[23] D. Vanderbilt, Phys. Rev. B **41**, 7892 (1990).
[24] H. J. Monkhorst and J. D. Pack, Phys. Rev. B **13**, 5188 (1976).
[25] M. J. Gillan, J. Phys.: Condens. Matter **1**, 689 (1989).
[26] L. V. Keldysh, Sov. Phys. JETP **20**, 1018 (1965).
[27] M. Büttiker, Y. Imry, R. Landauer, and S. Pinhas, Phys. Rev. B **31**, 6207 (1985).
[28] G. Taraschi, J.-L. Mozos, C. C. Wan, H. Guo, and J. Wang, Phys. Rev. B **58**, 13 138 (1998).
[29] H. Mehrez, A. Wlasenko, B. Larade, J. Taylor, P. Grutter, and H. Guo, Phys. Rev. B **65**, 195419 (2002).
[30] M. Brandbyge, J.-L. Mozos, P. Ordejon, J. Taylor, and K. Stokbro, Phys. Rev. B **65**, 165401 (2002).
[31] J. J. Palacios, A. J. Perez-Jimenez, E. Louis, E. SanFabian, and J. A. Verges, Phys. Rev. B **66**, 035322 (2002).
[32] J. Heurich, J. C. Cuevas, W. Wenzel, and G. Schön, Phys. Rev. Lett. **88**, 256803 (2002).
[33] J. Ortega, R. Perez, and F. Flores, J. Phys.: Condens. Matter **12**, L21 (2000).
[34] J. Ortega, Comput. Mater. Sci. **12**, 192 (1998).
[35] P. Jelinek, R. Prez, J. Ortega, and F. Flores, Phys. Rev. B **68**, 085403 (2003).
[36] A more detailed account of this mechanical instability will be published elsewhere.
[37] P. Dieska, I. Stich, and R. Perez, Phys. Rev. Lett. **91**, 216401 (2003).
[38] J. M. Pitarque, P. M. Echenique, and F. Flores, Surf. Sci. **217**, 267 (1989).
[39] J. Ferrer, A. Martín-Rodero, and F. Flores, Phys. Rev. B **38**, 10 113 (1988).
[40] R. Garcia and R. Perez, Surf. Sci. Rep. **47**, 197 (2002).